Materials Today Communications 31 (2022) 103323

Contents lists available at ScienceDirect

Materials Today Communications

journal homepage: www.elsevier.com/locate/mtcomm

Lattice dynamics and negative thermal expansion in layered mercury-based halides

Sushree Sarita Sahoo [a], Mayanak K. Gupta [b,c], Ranjan Mittal [b,c], G. Vaitheeswaran [d], V. Kanchana [a,*]

[a] Department of Physics, Indian Institute of Technology Hyderabad, Kandi 502285, Sangareddy, Telangana, India
[b] Solid State Physics Division, Bhabha Atomic Research Centre, Trombay, Mumbai 400085, India
[c] Homi Bhabha National Institute, Anushaktinagar, Mumbai 400094, India
[d] School of Physics, University of Hyderabad, Prof. C. R. Rao Road, Gachibowli, Hyderabad 500046, Telangana, India

ARTICLE INFO

Keywords:
Dynamical properties
Negative thermal expansion
Grüneisen parameters

ABSTRACT

Materials with negative thermal expansion are beneficial as they can be appropriately tuned to be compatible for device engineering. Here, we report our first-principles investigation on Hg_2X_2 and HgX_2 (X= Cl, I), which exhibits negative thermal expansion behaviour along c-direction. The first-principles studies reveal an anisotropic thermal expansion behaviour in the investigated compounds over a broad range of temperature. The computed coefficients along the c-axis are found to be negative for Hg_2Cl_2 and $HgCl_2$. Hg_2I_2 exhibits negative thermal expansion behaviour up to 100 K, while HgI_2 exhibits positive thermal expansion, whose values are qualitatively in good accord with the experimentally reported ones. The Grüneisen parameters along with elastic compliance matrix are used to calculate the thermal expansion coefficients of these materials. A detailed study of vibrational spectra was also done to get a better understanding of thermal expansion.

1. Introduction

The aberrant behaviour of materials when it contracts instead of expanding with the rise in temperature is defined as negative thermal expansion. Anharmonic lattice vibrations are the root cause of thermal expansion. Therefore, the vibrational frequency analysis of lattice vibrations and their volume dependence is necessary. Usually, phonon modes which strongly soften with pressure drive the negative thermal expansion [1,2]. There are numerous applications of these compounds and the most important one is tuning the expansion of a material to the desired value. For example, the thermal expansion of filling material should match the thermal expansion of teeth in dentistry. Similarly in different electronic devices the thermal expansion of each component should be tuned according to other components and the flow of electricity, to get maximum efficiency. Negative thermal expansion in solids has wide range of applications depending upon the range of temperature, like making high precision temperature devices, heat sinks, space crafts and satellites which gets exposed to a wide range of temperatures [3]. Hence, composites using negative thermal expansion materials to achieve zero thermal expansion have significant applications in different industrial sectors.

The detection of negative thermal expansion in ZrW_2O_8 over a broad range of temperature attracted the scientific community to explore more in this direction [4–10]. Similarly, other compounds like HfW_2O_8, ZrV_2O_7 and HfV_2O_7 also show large isotropic negative thermal expansion due to phonon softening [11,12]. Several ceramic and hybrid negative thermal expansion materials were also studied where the role of pressure-induced softening and transverse vibration of bridging atoms was taken into consideration [13]. Lattice dynamics and inelastic neutron scattering studies are vital tools for exploring negative thermal expansion. Using these techniques, alkaline earth fluorohalides MFX (M = Ba, Sr, Pb; X = Cl, Br, I) and aluminosilicate garnets $M_3Al_2Si_3O_{12}$(M = Ca, Mg, Mn and Fe) were also explored [2] and were found to have major application in different fields like, X-ray image storage, several device applications including storage devices, lasers, microwave optical elements and other industrial sectors. Similarly, mercury-based halides Hg_2X_2, HgX_2 (Cl, Br, I) were also explored for their various physical properties. Barta et al. reported the initial phase transition for Hg_2Cl_2 [14] in 1976, which was further examined experimentally using Brillouin scattering with an insight of exploring elastic properties for Hg_2Cl_2 [15]. The presence of very high anisotropic thermal conductivity and phonon scattering in Hg_2Cl_2 was studied in 1990 [16]. Roginkii et al. studied the Raman spectra and further pressure-dependent studies on Hg_2Cl_2 showed another phase transition at pressures greater than 9 GPa [17]. Anomalous X-ray transmission was also used to study the phase transition in Hg_2Cl_2 by Boiko

* Corresponding author.
E-mail address: kanchana@phy.iith.ac.in (V. Kanchana).

https://doi.org/10.1016/j.mtcomm.2022.103323
Received 21 December 2021; Received in revised form 12 February 2022; Accepted 19 February 2022
Available online 28 February 2022
2352-4928/© 2022 Elsevier Ltd. All rights reserved.

Table 1
Optimized parameters of Hg_2X_2, HgX_2 (where, X = Cl, Br and I) along with experimental parameters.

Compounds	Experimental parameters[a]				GGA+vdw				GGA				LDA			
	a(Å)	b(Å)	c(Å)	V(Å^3)	a(Å)	b(Å)	c(Å)	V(Å^3)	a(Å)	b(Å)	c(Å)	V(Å^3)	a(Å)	b(Å)	c(Å)	V(Å^3)
Hg_2Cl_2	4.47	–	10.88	217.83	4.54	–	11.01	226.79	4.75	–	11.09	250.16	4.28	–	10.94	200.32
Hg_2Br_2	4.66	–	11.33	241.75	4.72	–	11.29	251.52	4.94	–	11.35	277.23	4.46	–	11.15	221.38
Hg_2I_2	4.94	–	11.63	282.45	5.02	–	11.75	295.23	5.24	–	11.82	324.37	4.69	–	11.62	256.23
$HgCl_2$	12.76	5.97	4.33	330.09	12.79	6.07	4.2	348.64	13.85	6.76	4.27	399.54	13.29	5.76	3.89	298.02
$HgBr_2$	4.62	6.80	12.44	391.20	3.93	7.28	13.28	399.13	5.03	7.01	13.64	481.03	4.17	6.77	11.97	337.90
HgI_2	4.37	–	12.42	237.30	4.27	–	12.67	247.53	4.51	–	14.05	286.32	4.35	–	11.84	224.11

[a]Ref [19–22].

et al. [18]. The presence of negative thermal expansion was reported for Hg_2X_2 (Cl, Br, I) recently [19]. The linear structure along with presence of phase transitions induced by pressure and temperature in these mercurous halides made us curious to explore more about it. This work uses quasiharmonic approximations within the density functional theory to investigate negative thermal expansion by studying phonons, elastic properties, and dynamics of atoms in solids. The computational details are given in Section 2, analysis of results and discussion are given in Sections 3 and 4 concludes the paper with a brief summary.

Table 2
Mode assignment of Hg_2Cl_2.

No	Type	Modes	Frequency (cm^{-1})	Experimental (cm^{-1})[a]
1	Raman	E_g	34.9	40
2	IR	E_u	57.07	67
3	Raman	E_g	122.3	137
4	Raman	A_{1g}	151.62	167
5	IR	A_{2u}	224.99	254
6	Raman	A_{1g}	265.8	275

[a]Ref [17].

2. Computational details

The phonon calculations were performed using density functional theory implemented in Vienna Ab-initio Simulation Package (VASP) [23–25]. We have used GGA [26] and LDA [27] exchange correlation functional. The van der Waals interaction is also considered within DFT-D3 framework. The phonon calculation is performed on a geometrically optimized structure. The total energy minimization and geometry optimization were performed with a tolerance of 10^{-8} eV and 10^{-2} eV/Å respectively. The Monkhorst–Pack scheme [28] has been used to generate the special k-mesh in the Irreducible Brillouin Zone (IBZ). The Brillouin zone integration has been done using the tetrahedron method [29]. A planewave cut-off 900 eV has been used. The finite difference approach implemented in VASP were used for the elastic tensor calculations. The phonon calculations were performed using Phonopy [30]. For Hg_2X_2, a supercell of 4 × 4 × 2 is used for phonon calculations, whereas for $HgCl_2$ 2 × 3 × 4, for $HgBr_2$ 4 × 3 × 2 and for HgI_2 5 × 5 × 2 supercells were used.

The thermal expansion calculations have been performed within quasi-harmonic approximation using Eqs. (1)–(2). The Grüneisen parameters have been calculated by applying a strain along *i*th direction as described by Eq. (3). The Grüneisen parameters along with elastic compliance matrix values are used to calculate the linear thermal expansion coefficients. The equations for calculating thermal expansion coefficients (α) along 'a' and 'c' directions for a tetragonal system are [31]:

$$\alpha_a = \sum_{q,j}(C_V(q,j,T)/V)[(S_{11}+S_{12})\Gamma_a + S_{13}\Gamma_c]$$
$$\alpha_c = \sum_{q,j}(C_V(q,j,T)/V)[2S_{13}\Gamma_a + S_{33}\Gamma_c] \quad (1)$$

Similarly for orthorhombic system the equations are [32]:

$$\alpha_a = \sum_{q,j}(C_V(q,j,T)/V)[S_{11}\Gamma_a + S_{12}\Gamma_b + S_{13}\Gamma_c]$$
$$\alpha_b = \sum_{q,j}(C_V(q,j,T)/V)[S_{21}\Gamma_a + S_{22}\Gamma_b + S_{23}\Gamma_c] \quad (2)$$
$$\alpha_c = \sum_{q,j}(C_V(q,j,T)/V)[S_{31}\Gamma_a + S_{32}\Gamma_b + S_{33}\Gamma_c]$$

The mode Grüneisen parameter of phonon energy $E_{q,j}$ is given as [32],

$$\Gamma_l(E_{q,j}) = -(\frac{\partial lnE_{q,j}}{\partial lnl}); l, l' = a, b, c; l' \neq l \quad (3)$$

Here, Γ represent the Grüneisen parameter components along different directions, S represents the components of elastic compliance matrix tensor, V is the unitcell volume and C_V(q, j, T) is the specific heat contribution from the phonon of energy E_{qj} that is energy of *j*th phonon mode at point q in Brillouin zone. Using the above equations, we have calculated the coefficients of thermal expansion for the investigated compounds.

3. Results and discussions

3.1. Mechanical and dynamical properties

The compounds Hg_2X_2 (X = Cl, Br, I) crystallize in tetragonal phase with space group *I4/mmm* (139), whereas in HgX_2 (X = Cl, Br, I), $HgCl_2$ and $HgBr_2$ both crystallize in orthorhombic phase with space group *Pnma*(62) and *Cmc21*(36) respectively, while HgI_2 crystallize in tetragonal phase with space group *P42/nmc*(137). The optimization was done using generalized gradient approximation (GGA) with and without the inclusion of van der Waals interaction (DFT-D3 method of Grimme). Table 1 shows that the optimized parameters obtained using GGA+vdw are in good agreement with the experimentally reported values [19–22]. In Fig. 2 we have shown the calculated phonon dispersions for Hg_2X_2 and HgX_2 along several high-symmetry directions. The computed dispersion shows the presence of very low energy acoustic and optical modes in all these compounds, which indicates that the investigated compounds are strongly anharmonic systems. Though the harmonic approximation does not work for the strongly anharmonic systems, it can give the sign of the strong anharmonicity of the materials to some extent, such as imaginary phonon frequencies. Due to the limitations of calculations these strong anharmonicity could not be captured well. This anharmonicity usually arises due to large lattice vibration amplitude which could induce the negative thermal expansion [33]. We have also computed the atomic contribution of different element to total phonon density of states (Fig. 3). At low energy states up to 10 meV, Hg-atoms are contributing most to phonon spectra. Above 10 meV, both halides and mercury atoms contribute to the entire range of phonon spectrum. At high energy phonon spectrum, the contribution of halide atoms is decreasing with mass number of X in Hg_2X_2 series. This is an expected behaviour due to renormalization of phonon frequencies due to masses of X (Cl, Br, I) atoms. Further, the maximum range of phonon spectra is found to decrease as we go from the lighter(Cl) to heavier atom(I). A similar trend is observed in HgX_2 series at low energy states, whereas at high energies, the halide atoms are dominating. We have explored the irreducible representations of phonon modes to get more details, and also compared our theoretical

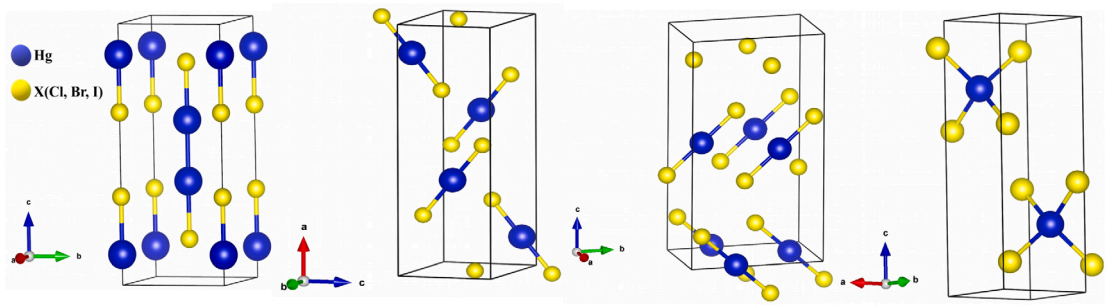

Fig. 1. Crystal structure of (a) Hg_2Cl_2 (b) $HgCl_2$ (c) $HgBr_2$ (d) HgI_2.

Table 3
Elastic constants of HgX_2, (X:Cl,Br,I).

Compound/Elastic constants	$HgCl_2$	HgI_2	HgI_2(exp)[a]
C_{11} (GPa)	23.116	30.670	33.03
C_{12} (GPa)	3.646	4.409	5.59
C_{13} (GPa)	10.284	10.843	11.68
C_{22} (GPa)	16.731	30.670	33.03
C_{23} (GPa)	8.666	10.843	11.68
C_{33} (GPa)	13.4	15.679	16.34
C_{44} (GPa)	7.714	6.426	7.23
C_{55} (GPa)	5.981	6.426	7.23
C_{66} (GPa)	0.907	1.844	2.31
Bulk Modulus (GPa)	10.828	14.004	–
Young's modulus (GPa)	10.021	13.988	–
Shear Modulus (GPa)	3.723	5.245	–
Poisson's ratio (ν)	0.346	0.334	–

[a]Ref [35].

Table 4
Elastic properties of Hg_2X_2, (X: Cl,I).

Compound/Elastic properties	Hg_2Cl_2	Hg_2Cl_2 [exp][a]	Hg_2I_2
C_{11} (GPa)	17.518	18.75	10.3
C_{12} (GPa)	17.783	17.10	11.14
C_{13} (GPa)	14.558	15.64	7.69
C_{33} (GPa)	88.075	80.10	97.75
C_{44} (GPa)	−55.611	8.55	4.006
C_{66} (GPa)	16.319	12.85	11.794

[a]Ref [15].

Table 5
Elastic compliance values of Hg_2X_2, HgX_2, (X:Cl,I).

Compound/Elastic properties	Hg_2Cl_2	Hg_2I_2	$HgCl_2$	HgI_2
S_{11} (GPa^{-1})	−1.87	−0.57	0.0694	0.044
S_{12} (GPa^{-1})	1.90	0.62	0.0268	0.006
S_{13} (GPa^{-1})	−0.005	−0.004	−0.0654	−0.0344
S_{22} (GPa^{-1})	−1.87	−0.57	0.0949	0.044
S_{23} (GPa^{-1})	−0.005	−0.004	−0.076	−0.0344
S_{33} (GPa^{-1})	0.0131	0.011	0.1738	0.1114

results with the previously available experimental Raman or Infrared data which are given in Table 2, Supplementary material Table 1-5. All the investigated compounds are very soft in nature and the phonon dispersion curves can change drastically with volume. The volume difference with GGA exchange correlation functional without considering van der Waals effect is around 14% for Hg_2Cl_2 [Table 1]. This system is dynamically stable using GGA parameters as all the phonon mode frequencies are positive, (Supplementary Figure: (A)) and it agrees well with the recently reported results by R. Li et al. [34]. Since, we observe a 14% volume change with GGA functional which is not admissible for consistency with experiments, we have included van der Waals effect for further study.

To study the effect of size of halide ions in thermal expansion, we have taken X: Cl and I, for further investigation. Elastic constant as well as elastic compliance have been calculated (Tables 3–5). The elastic compliance matrix is calculated by taking the inverse of elastic constant matrix i.e., $S = C^{-1}$ [36,37]. We got six and nine non-equivalent elastic constants for tetragonal systems (Hg_2Cl_2, Hg_2I_2, HgI_2) and orthorhombic system ($HgCl_2$) which are given in Tables 3, 4. The compounds $HgCl_2$ and HgI_2 satisfy the Born stability criteria and are mechanically stable at zero temperature. From Table 3, it is found that the elastic constant C_{44} is negative for Hg_2Cl_2 and also the experimental value of C_{44} for Hg_2Cl_2 is very low in comparison to other elastic constants. We find that all other elastic constants, except for C_{44} are in good agreement with the experimentally reported ones [15]. The investigated compounds Hg_2Cl_2 and Hg_2I_2 have linear structure similar to MCN (M: Cu, Ag, Au) where the bonding nature was discussed through the difference in elastic constants C_{11} and C_{33}[38]. The linear structure provides more flexibility which favours bending motion in the direction perpendicular to the linear chain (in the ab-plane). The large difference seen in the C_{11} and C_{33} of Hg_2Cl_2 and Hg_2I_2 (Table 4) indicates the difference in the nature of bonding along c-direction and ab-plane. The large value of C_{33} among all the three Hg_2X_2 compounds infers that the linear bonding of X–Hg–Hg–X along c-direction is strongest in Hg_2I_2 in comparison to other compounds. The large value of C_{33} along with the difference in ionic radii between halides and mercury atom indicates that Hg_2I_2 does not expand easily along c-direction and gets distorted with the application of temperature in comparison to other compounds in that series.

3.2. Thermal expansion in Hg_2X_2, (X = Cl,I)

From the phonon spectra of Hg_2Cl_2, we found that one of the lower acoustic phonon modes become unstable. This might indicate the presence of another lower symmetry phase at 0 K, which is consistent with earlier reported structural phase transition at 186 K from tetragonal to orthorhombic phase [17]. The crystal structure of Hg_2X_2 is shown in Fig. 1(a). The bending of Cl–Hg–Hg–Cl bond chain with the increase of temperature, leads to change in the volume of unit cell, which further results in phase transition [18]. The phonon dispersion curve for Hg_2Cl_2 is shown in Fig. 2. Softening of phonon mode in the Γ-X direction is observed in this compound. At low temperature the acoustic and low energy optical modes dominate as they get excited easily. The *I4/mmm* space group for Hg_2Cl_2 has one formula unit (4 atoms) in primitive cell. This would result in 12 phonon modes. The group-theoretical decomposition of phonons at the zone centre is given as:

$$\Gamma = 2E_u + 2A_{2u} + 2E_g + 2A_{1g}$$

Here E_u and E_g are doubly degenerate modes and rest are singly degenerate modes. From the above-mentioned modes, $1E_u$ and 1 A_{2u} modes are acoustic modes and the other $1E_u$, 1 A_{2u} are infra-red active modes. E_g and A_{1g} are Raman active phonon modes. The measured

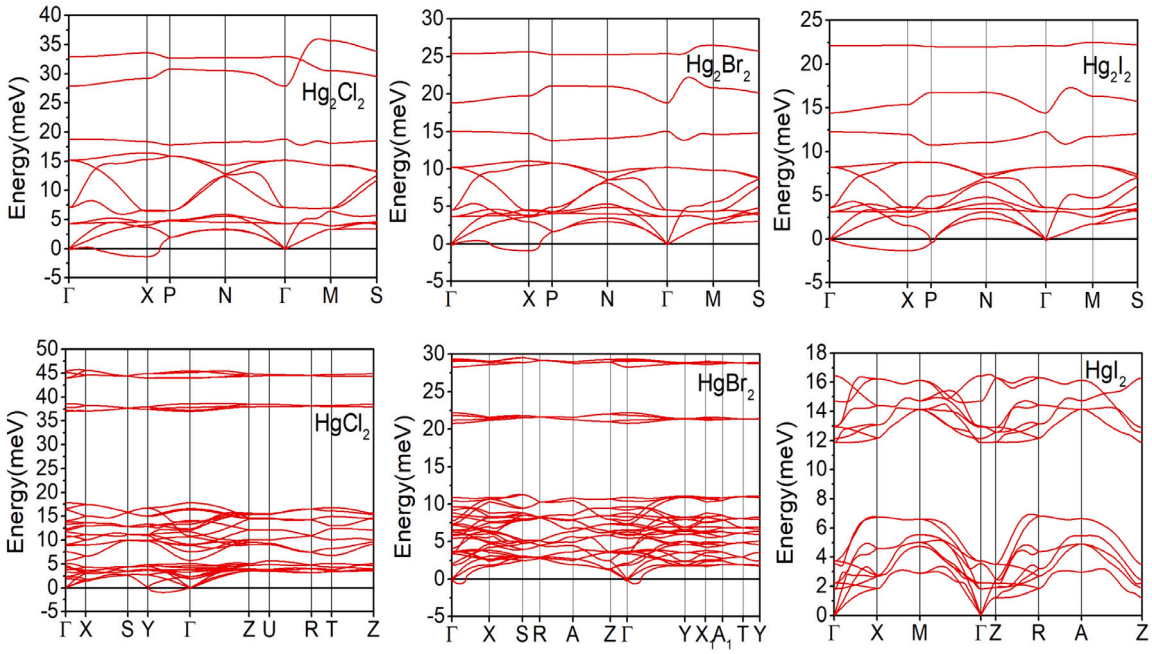

Fig. 2. Phonon dispersion curves calculated at optimized lattice constants.

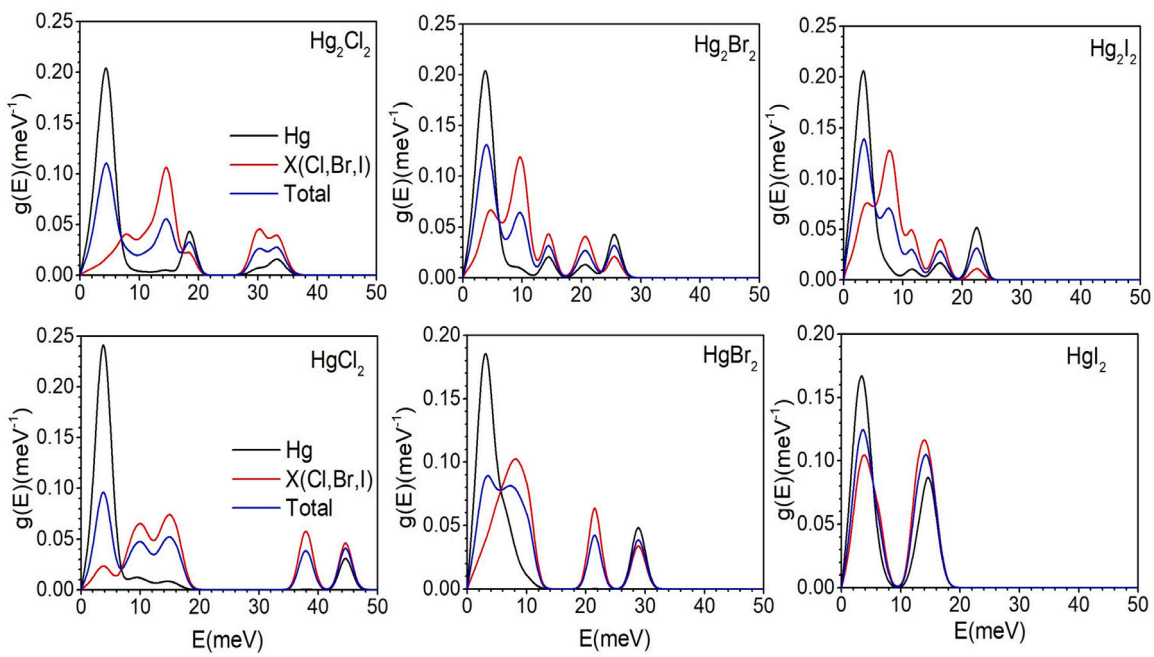

Fig. 3. Partial phonon density of states of compounds and its constituent atoms.

positive frequencies matches well with the experimentally measured values [17]. Mode representations are shown in Fig. 6.

From the vibrational frequencies tabulated in Table 2, the E_g modes with frequency 34.9 cm^{-1}, represent the rocking of the linear molecule as a whole. The E_g modes with frequency 122.3 cm^{-1} corresponds to zigzag bending vibrations. The last 3 modes are dominated by Hg–Hg and Hg–Cl stretching vibrations. The anharmonic vibrations in ab-plane may enhance the distortion in the plane, which could lead to the reduction in the c-lattice parameter with temperature. Basically, the high amplitude transverse vibrations of atoms result in bending of linear structure, which contribute to both positive thermal expansion in the ab-plane and negative thermal expansion along c-direction [39]. The negative phonon mode, phonon softening and reported phase transition indicate the possibility for the negative thermal expansion in Hg_2Cl_2. Similarly, Hg_2I_2 also undergoes a phase transition from body-centred tetragonal to an orthorhombic structure at 9 Kbar pressure at 300 K and reported to have negative thermal expansion below 100 K which is also confirmed by our calculations [40]. Further, we are interested to see the effect of change in ionic radii on the thermal expansion calculations. The detailed calculations for thermal expansion are done only for Hg_2Cl_2 and Hg_2I_2 (Figs. 4, 5). The calculated anisotropic mode Grüneisen parameters Γ_a and Γ_c (Fig. 4(a)) averaged over all the phonons in the entire Brillouin zone as a function of phonon energy shows that the magnitude of negative Γ_c for Hg_2Cl_2 is larger in comparison to that in Hg_2I_2. The calculated Grüneisen parameters and

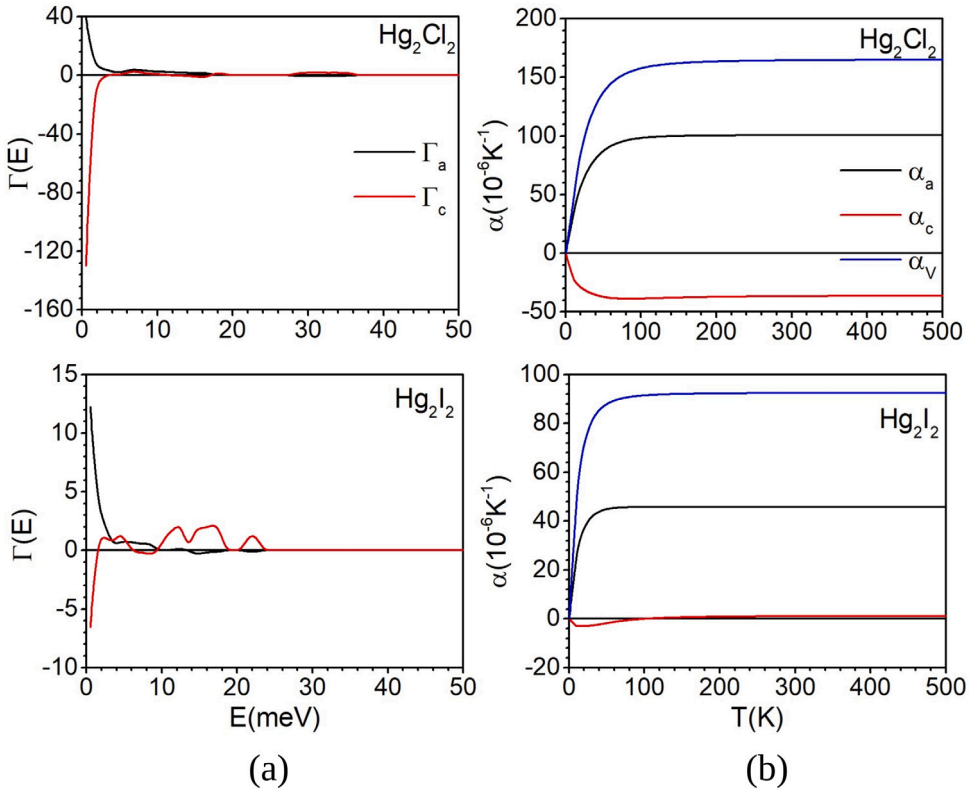

Fig. 4. (a) Calculated Grüneisen parameters of various atoms as a function of phonon energy for Hg_2X_2 series. (b) Calculated linear and volume thermal expansion coefficients as a function of temperature.

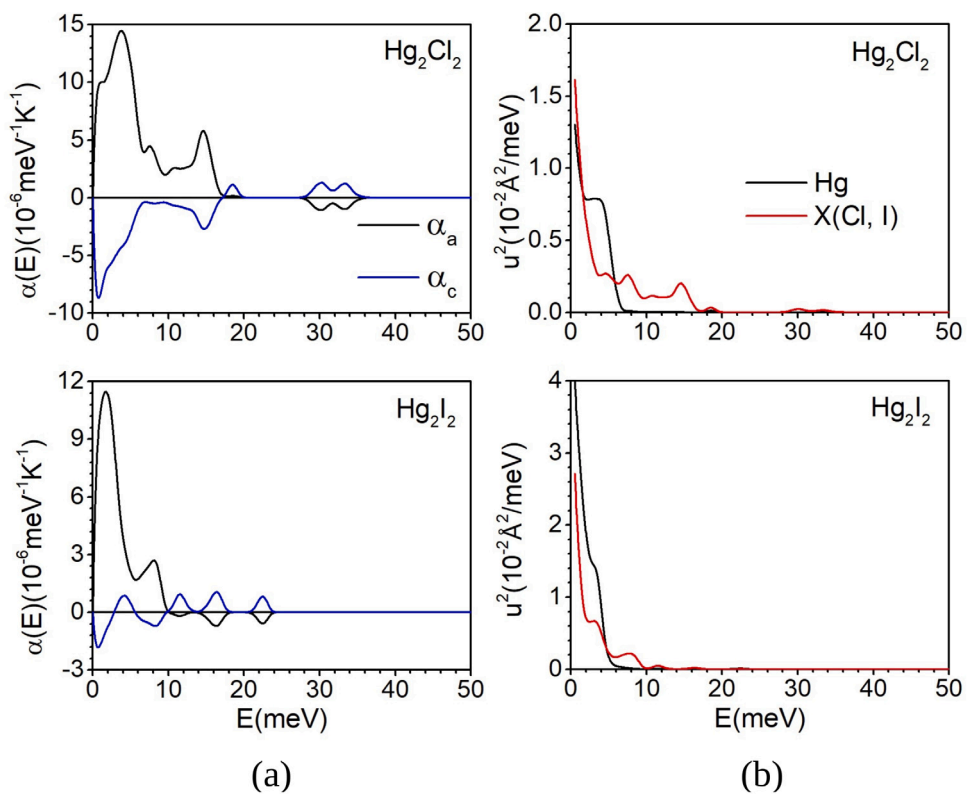

Fig. 5. (a) The contribution to anisotropic linear thermal expansion coefficients at 300 K, from phonon modes of energy E averaged over Brillouin zone. (b) The contribution of phonons of energy E to the mean-squared amplitude of various atoms for Hg_2X_2 series at 300 K.

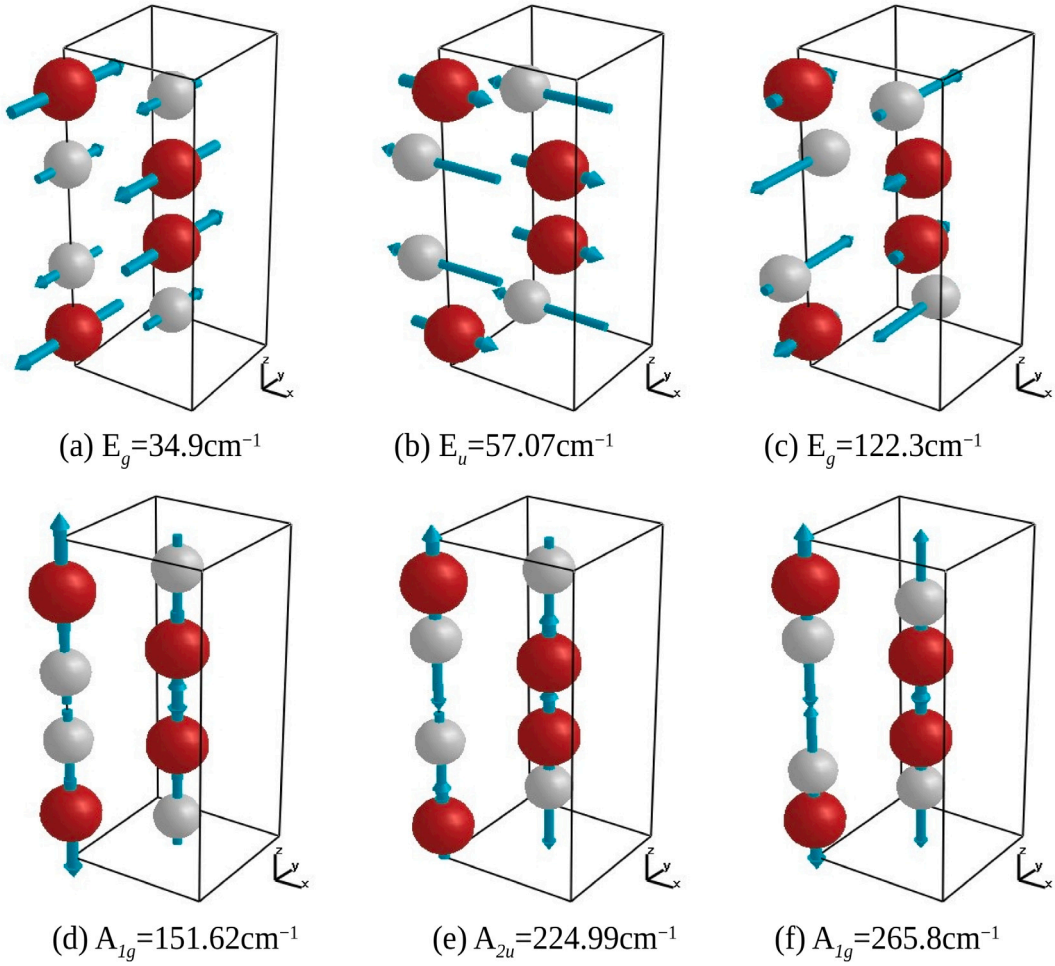

Fig. 6. Hg_2Cl_2 mode representations.

Table 6
Negative thermal expansion values of Hg_2X_2, HgX_2 (where, X = Cl, I).

Negative thermal expansion values		Hg_2Cl_2	Hg_2I_2	$HgCl_2$	HgI_2
$\alpha_a(\times10^{-6})$ K^{-1}	Experimental	68.60[a]	59.80[a]	–	12.00[b]
	Calculated	100.60	45.65	645.00	1.80
$\alpha_b(\times10^{-6})$ K^{-1}	Experimental	–	–	–	–
	Calculated	–	–	179.10	–
$\alpha_c(\times10^{-6})$ K^{-1}	Experimental	−4.40[a]	−4.20[a]	–	25.00[b]
	Calculated	−36.60	1.04	−452.50	19.40

[a]Ref [19].
[b]Ref [41].

the elastic compliance values (Table 5) are used to calculate anisotropic coefficients of thermal expansion.

In Hg_2Cl_2 negative thermal expansion is seen in the c-direction. The experimentally reported values [19] of average thermal expansion coefficients from high temperature X-ray diffraction measurements in the temperature range from 300 K to 450 K are $\alpha_a = 68.6 \times 10^{-6}$ K^{-1} and $\alpha_c = -4.4 \times 10^{-6}$ K^{-1}. Our calculated thermal expansion coefficients along a- and c- directions averaged within 300 K to 450 K are 100.6×10^{-6} K^{-1} and -36.7×10^{-6} K^{-1} respectively. For Hg_2I_2 experimentally negative thermal expansion is observed along c-direction with $\alpha_c = -4.2 \times 10^{-6}$ K^{-1} [19], but we find that our calculations show negative thermal expansion behaviour along *c*-axis only below 100 K. At higher temperatures (100 K to 500 K) our calculations show positive thermal expansion coefficient ($\alpha_c = 1.04 \times 10^{-6}$ K^{-1}). The calculated average value of α_a (45.68×10^{-6} K^{-1}) agrees with the experimental value of 59.8×10^{-6} K^{-1}[19] (Table 6). The discrepancy between calculated and measured expansion behaviour could be attributed to a strong anharmonic transverse phonon, which could not be well captured in the quasiharmonic approximation. Hence, the agreement between the computed and experimental values of thermal expansion coefficient in both the compounds should be considered good, as calculations show that these compounds are very soft. Our calculations are useful to understand thermal expansion behaviour in these compounds qualitatively.

We further computed the contribution of phonons with energy E, to the thermal expansion coefficients at 300 K and are shown in Fig. 5(a). In both the compounds, phonons of energy about 2 meV contribute maximum to both positive expansion in ab-plane and negative thermal expansion along *c*-axis. These modes are mostly dominated by transverse dynamics of Hg-X chain in Hg_2Cl_2. In Hg_2Cl_2 we find that phonons of energy up to 15 meV contribute to the thermal expansion behaviour, while in Hg_2I_2 the energy of phonons which contribute

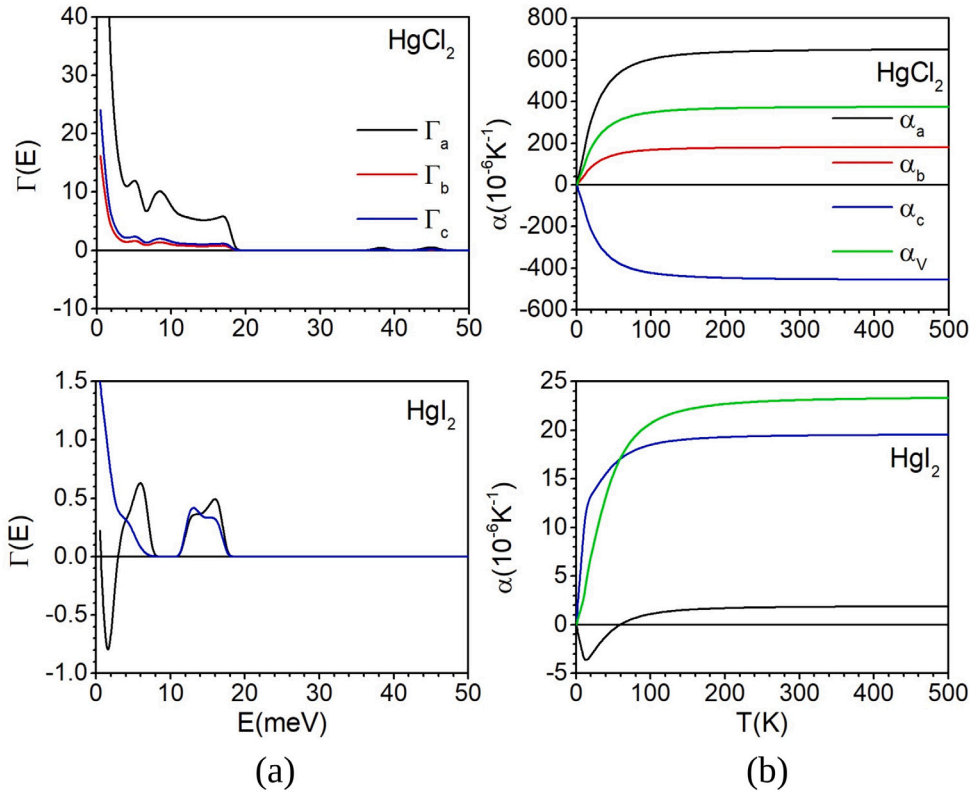

Fig. 7. (a) Calculated Grüneisen parameters of various atoms as a function of phonon energy for HgX_2 series. (b) Calculated linear and volume thermal expansion coefficients as a function of temperature.

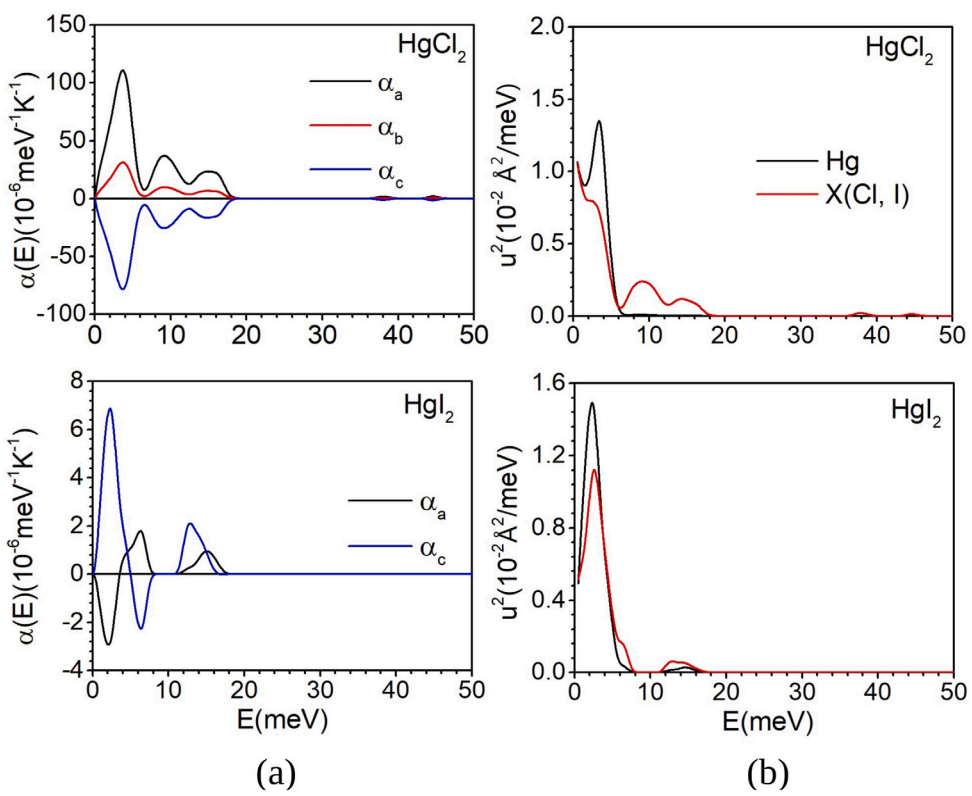

Fig. 8. (a) The contribution to anisotropic linear thermal expansion coefficients at 300 K, from phonon modes of energy E averaged over Brillouin zone. (b) The contribution of phonons of energy E to the mean-squared amplitude of various atoms for HgX_2 series at 300 K.

significantly to thermal expansion are below 10 meV. The calculated partial phonon density of states shows (Fig. 3) that due to the heavier mass the iodine dynamics contribution occurs at lower energies in comparison to that of chlorine. These higher energy modes which contribute significantly to thermal expansion mainly have contributions from X (Cl, I) atoms. The contribution of phonons to thermal expansion can also be understood from mean-squared displacements (u^2) dependence on phonon energy. In Fig. 5(b), we have shown the u^2 as a function of phonon energy, E averaged over Brillouin zone at 300 K. The low-energy modes below 2 meV, show large contribution to the mean-squared displacement. These low-energy modes involve vibrations of both Hg and X (Cl, I) elements. While higher energy vibration has dominant contribution from X (Cl, I) elements. These low-energy modes below 2 meV possess long-wave transverse dynamic character along (001) (Fig. 2), creates the larger transverse displacement in Hg-X chains, results in negative thermal expansion along c-axis. Supplementary Figure:(B) gives the plots for specific heats for Hg_2Cl_2 and Hg_2I_2. The specific heat first increases with temperature and eventually becomes constant for all the compounds. At high temperatures the value of C_P is larger than the value of C_V due to the large value of thermal expansion coefficients ($C_P - C_V = \alpha_V^2 BVT$, 'B' is isothermal bulk modulus and 'V' and 'T' are the volume and the temperature).

3.3. Thermal expansion in HgX_2, (X:Cl,I)

Similar to Hg_2X_2, few other mercury-based halides (HgX_2; X = Cl, I) are also studied and they also host the possibility of negative thermal expansion in them, which is discussed here in detail. The crystal structure of HgX_2 compounds are shown in Fig. 1(b–d). The phonon dispersion curve for $HgCl_2$ is shown in Fig. 2. The group-theoretical decomposition of phonons at the zone-centre is given as:

$$\Gamma = 3B_{2u} + 6B_{3u} + 6B_{1u} + 3A_u + 6A_g + 3B_{3g} + 6B_{2g} + 3B_{1g}$$

Here, $1B_{2u}$, $1B_{3u}$ and $1B_{1u}$ are acoustic modes and the rest are optic modes. Among the optic modes, $2B_{2u}$,$5B_{3u}$,$5B_{1u}$ are infra-red active, $6A_g$, $3B_{1g}$, $6B_{2g}$ and $3B_{3g}$ are Raman active and $3A_u$ are silent modes. The detailed mode assignment along with experimental comparison is given is supplementary material Table 5. The phonon dispersion curve of this compound shows negative phonon frequencies along the Y-Γ direction which is caused by the vibration of low energy B_{2u} infra-red active phonon mode. For HgI_2 phonon dispersion is shown in Fig. 2. The group-theoretical decomposition of phonons at the zone-centre is given as:

$$\Gamma = 3E_u + 2A_{2u} + 3E_g + 2B_{1g} + B_{2u} + A_{1g}$$

Here, $1E_u$ and 1 A_{2u} are acoustic, $2E_u$, $1A_{2u}$ are infra-red active, $3E_g$, $2B_{1g}$, A_{1g} are Raman active and B_{2u} mode is inactive. There is a softening of acoustic E_u mode in phonon dispersion curve along Γ-Z direction as shown in Fig. 2. The phonon dispersion curve and the elastic constants show the dynamical and mechanical stability of the compound.

The calculated thermal expansion behaviour for $HgCl_2$ and HgI_2 are shown in Figs. 7, 8. It may be noted that experimental data [41] is only available for HgI_2. From Fig. 7 we can infer that, low energy phonon modes below 2 meV in HgI_2 contribute towards the slight negative Γ_a value, while phonons of same energy also contribute towards the positive Γ_c values. The elastic compliance values (Table 5) along with the Γ_a and Γ_c values give us the thermal expansion behaviour as shown in Fig. 7. The linear thermal expansion coefficients as a function of phonon energy at 300 K is shown in Fig. 8(a). It may be noted that low energy modes below 4 meV contribute to negative values to α_a, while the positive contribution from high energy modes results in overall positive values. The calculated phonon spectra show (Fig. 4) that at these low energy modes Hg atoms has slightly more contributions in comparison to I atoms. The structure of $HgCl_2$ is orthorhombic. The calculated anisotropic Grüneisen parameter values for $HgCl_2$ have large positive values. The calculated anisotropic thermal expansion values at 300 K are $\alpha_a = 645.0 \times 10^{-6}$ K^{-1}, $\alpha_b = 179.1 \times 10^{-6}$ K^{-1}, $\alpha_c = -452.5 \times 10^{-6}$ K^{-1} (Table 6). The calculated bulk modulus values (Table 3) for $HgCl_2$ and HgI_2 are found to 10.8 GPa and 14.0 GPa, respectively. As the investigated compounds have very low bulk modulus, so the pressure dependence of modes may not have been accurately calculated, which leads to overestimation of calculated negative thermal expansion behaviour and results in high values of thermal expansion coefficients. It may be noted that all the anisotropic Grüneisen parameters have positive values in $HgCl_2$. However, the negative value of S_{31} (=S_{13}) along with the large positive value of Γ_a, result in negative α_c. The linear thermal expansion coefficient values for $HgCl_2$ are found to be 10 times larger in comparison to HgI_2. This may be due to the fact that, $HgCl_2$ is softer in comparison to that of HgI_2. The calculated contribution to linear thermal expansion coefficients from phonon of energy E at 300 K (Fig. 8(a)) shows that modes below 6 meV contribute mainly to linear thermal expansion coefficients. It can be seen that at these energies, Hg atoms (Fig. 3) has more contribution in comparison to Cl atoms. In both $HgCl_2$ and HgI_2 compounds, the phonon contribution to mean-squared displacement, shows dominant contribution from modes below 6 meV. Further, we found that Hg have larger contribution than X (Cl, I) unlike the case of Hg_2X_2. Here also these low energy modes mainly show the transverse vibration of HgX_4 polyhedral units. Specific heat curves of the compounds (Supplementary Figure: (C)) in HgX_2 series have lower values as compared to compounds of Hg_2X_2 series but a similar trend is observed in both series.

The crystal symmetry changes when we go down in the halogen group from Cl to I in HgX_2, along with different oxidation states of Hg (+2 in HgX_2 and +1 in Hg_2X_2), so the trend of the negative thermal expansion cannot be compared. From the other series of compounds HgX_2, $HgCl_2$ shows maximum thermal expansion followed by HgI_2. But these compounds are not explored so far experimentally and await further verification.

4. Conclusion

In summary, a strong negative thermal expansion is observed in Hg_2Cl_2 (-36.7×10^{-6} K^{-1} along c-axis), $HgCl_2$ (-452.5×10^{-6} K^{-1} along c-axis) at room temperature. Positive thermal expansion is found along a and b axis resulting in overall positive volume thermal expansion. Hg_2I_2 is experimentally reported to have negative thermal expansion till 100 K which agrees well with our calculations. Other thermodynamic properties such as phonon density of states, vibrational properties and specific heats have been studies as well. We have also discussed the relation between elastic constants and thermal expansion, implying that even positive Grüneisen parameters can also results in negative thermal expansion. These axis-dependent negative thermal expansion properties have a diverse application in electronic and optical devices, space, and thermo-mechanical engineering industries. The other compounds in the series are also open for further exploration in this direction.

CRediT authorship contribution statement

Sushree Sarita Sahoo: Executing the problem, Running the calculations, Data analysis, Manuscript preparation. **Mayanak K. Gupta:** Running a part of calculations, Analysis of results, Editing the manuscript, Discussion. **Ranjan Mittal:** Running a part of calculations, Analysis, Manuscript editing, Validation. **G. Vaitheeswaran:** Problem Identification, Discussion of results, Editing manuscript. **V. Kanchana:** Problem Identification, Data analysis, Discussion of results, Manuscript preparation and editing, Supervision.

Declaration of competing interest

The authors declare that they have no known competing financial interests or personal relationships that could have appeared to influence the work reported in this paper.

Data availability

Data generated in this work is available upon request.

Acknowledgements

The authors Sushree Sarita Sahoo and V. Kanchana acknowledge IIT Hyderabad for providing computational facilities and CSIR project with sanction No. (03(1433)/18/EMR-II) for financial support. G.V would like acknowledge UoH-IoE-RC3-21-046 for funding and CMSD University of Hyderabad for providing the computational facility. G.V would like to acknowledge Dr. Priyanthi Amarasinghe and Dr. Syed B. Qadri for sharing the experimental details of Hg_2X_2 compounds.

Appendix A. Supplementary data

Supplementary material related to this article can be found online at https://doi.org/10.1016/j.mtcomm.2022.103323.

References

[1] M.T. Dove, H. Fang, Rep. Progr. Phys. 79 (6) (2016) 066503.
[2] R. Mittal, S. Chaplot, N. Choudhury, Prog. Mater. Sci. 51 (2) (2006) 211–286.
[3] J.S.O. Evans, J. Chem. Soc. Dalton Trans. (1993) 3317–3326.
[4] T.A. Mary, J.S.O. Evans, T. Vogt, A.W. Sleight, Amer. Assoc. Adv. Sci. 272 (5258) (1996) 90–92.
[5] J.S.O. Evans, T.A. Mary, T. Vogt, M.A. Subramanian, A.W. Sleight, Chem. Mater. 8 (12) (1996) 2809–2823.
[6] J.S.O. Evans, W.I.F. David, A.W. Sleight, Acta Crystallogr. B 55 (3) (1999) 333–340.
[7] G. Ernst, C. Broholm, G.R. Kowach, A.P. Ramirez, Nature 396 (1998) 147–149.
[8] A.P. Ramirez, G.R. Kowach, Phys. Rev. Lett. 80 (1998) 4903–4906.
[9] C.A. Kennedy, M.A. White, Solid State Commun. 134 (4) (2005) 271–276.
[10] D. Cao, F. Bridges, G.R. Kowach, A.P. Ramirez, Phys. Rev. Lett. 89 (2002) 215902.
[11] R. Mittal, S.L. Chaplot, A.I. Kolesnikov, C.K. Loong, T.A. Mary, Phys. Rev. B 68 (2003) 054302.
[12] R. Mittal, S.L. Chaplot, Phys. Rev. B 78 (2008) 174303.
[13] H. Fang, M.T. Dove, A.E. Phillips, Phys. Rev. B 89 (2014) 214103.
[14] C. Barta, J.P. Chapelle, G. Hauret, Cao Xuan An, A. Fouskova, C. Konak, Phys. Status Solidi (A) (1976) 34.
[15] C. Xuan An, G. Hauret, J. Chapelle, Solid State Commun. 24 (6) (1977) 443–445.
[16] M.B. Koss, K.A. McCarthy, H.H. Sample, Phys. Rev. B 42 (1990) 5822–5833.
[17] E. Roginskii, A. Krylov, Y. Markov, M. Smirnov, Bull. Russ. Acad. Sci.: Phys. 80 (2016) 1033–1037.
[18] M.E. Boiko, M.D. Sharkov, A.M. Boiko, S.G. Konnikov, Crystallogr. Rep. 63 (2) (2018) 196–199.
[19] P.M. Amarasinghe, Joo-Soo Kim, S. Trivedi, S.B. Qadri, E.P. Gorzkowski, G. Imler, J. Soos, N. Gupta, J. Jensen, J. Electron. Mater. 48 (2019) 7063–7067.
[20] S. Karmakar, S.M. Sharma, Solid State Commun. 131 (7) (2004) 473–478.
[21] V. Subramanian, K. Seff, Acta Crystallogr. B 36 (9) (1980) 2132–2135.
[22] Haakon Braekken, Kristallogr.-Cryst. Mater. 81 (1–6) (1932) 152–154.
[23] G. Kresse, J. Furthmuller, Comput. Mater. Sci. 6 (1) (1996) 15–50.
[24] G. Kresse, J. Furthmuller, Phys. Rev. B 54 (16) (1996) 11169.
[25] G. Kresse, D. Joubert, Phys. Rev. B 59 (3) (1999) 1758.
[26] J.P. Perdew, K. Burke, M. Ernzerhof, Phys. Rev. Lett. 77 (18) (1996) 3865.
[27] R.G. Parr, W. Yang, Int. J. Quantum Chem. 47 (1) (1993) 101.
[28] H.J. Monkhorst, J.D. Pack, Phys. Rev. B 13 (12) (1976) 5188.
[29] P. Blochl, O. Jepsen, O. Andersen, Phys. Rev. B 49 (1994) 16223–16233.
[30] A. Togo, F. Oba, I. Tanaka, Phys. Rev. B 78 (2008) 134106.
[31] E.T. Ritz, N.A. Benedek, Phys. Rev. Lett. 121 (2018) 255901.
[32] P. Goel, M.K. Gupta, S.K. Mishra, B. Singh, R. Mittal, S.L. Chaplot, Front. Chem. 6 (2018) 331.
[33] . Wei, B. Wei, Q. Sun, C. Li, J. Hong, Sci. China Phys. Mech. Astron. 64 (2021) 1869–1927.
[34] Rongzhen Li, Guodong Zhang, Lin Liu, Longzhen Zhang, Peng Zhang, Xiang Li, Yuniq Hua, Xutang Tao, Comput. Mater. Sci. 188 (2021) 110139.
[35] S. Haussuhl, H. SaHoLz, Krist. Tech. 10 (11) (1975) 1175–1179.
[36] S. Wu, S. Shahab Naghavi, G.H. Fecher, C. Felser, J. Mod. Phys. 9 (2018) 775–805.
[37] S. Ozdemir Kart, T. Cagn, J. Alloys Compd. 508 (1) (2010) 177–183.
[38] M.K. Gupta, B. Singh, R. Mittal, S. Rols, S.L. Chaplot, Phys. Rev. B 93 (2016) 134307.
[39] M.K. Gupta, B. Singh, R. Mittal, M. Zbiri, A.B. Cairns, A.L. Goodwin, H. Schober, S.L. Chaplot, Phys. Rev. B 96 (2017) 214303.
[40] C.A. Occhialini, S.U. Handunkanda, A. Said, S. Trivedi, G.G. Guzmn-Verri, J.N. Hancock, Phys. Rev. Mater. 1 (2017) 070603.
[41] N.V. Long, K. Kleinstueck, J. Tobisch, P. Klinger, K. Prokert, V. Schuricht, Cryst. Res. Technol. 18 (1983) K93–K97.